

# Visual Forecasting of Time Series with Image-to-Image Regression

Naftali Cohen, Srijan Sood, Zhen Zeng, Tucker Balch, and Manuela Veloso

J. P. Morgan AI Research

naftali.cohen@jpmchase.com, srijan.sood@jpmchase.com, zhen.zeng@jpmchase.com,  
tucker.balch@jpmchase.com, manuela.veloso@jpmchase.com

## Abstract

*Time series forecasting is essential for agents to make decisions in many domains. Existing models rely on classical statistical methods to predict future values based on previously observed numerical information. Yet, practitioners often rely on visualizations such as charts and plots to reason about their predictions. Inspired by the end-users, we re-imagine the topic by creating a framework to produce visual forecasts, similar to the way humans intuitively do.*

*In this work, we take a novel approach by leveraging advances in deep learning to extend the field of time series forecasting to a visual setting. We do this by transforming the numerical analysis problem into the computer vision domain. Using visualizations of time series data as input, we train a convolutional autoencoder to produce corresponding visual forecasts.*

*We examine various synthetic and real datasets with diverse degrees of complexity. Our experiments show that visual forecasting is effective for cyclic data but somewhat less for irregular data such as stock price. Importantly, we find the proposed visual forecasting method to outperform numerical baselines. We attribute the success of the visual forecasting approach to the fact that we convert the continuous numerical regression problem into a discrete domain with quantization of the continuous target signal into pixel space.*

## 1. Introduction

Time series forecasting has been extensively studied in statistical literature that uses historical information to predict future values. The underlying assumption is that past information contains signals that are expected to continue (e.g., [21]). Over the years, many techniques have been developed for point-wise forecasting and confidence intervals about the prediction. The vast majority of successful forecasting algorithms use traditional statistical ideas (e.g., [39, 21, 22]). Some are simplistic, based on rolling averages, while some involve more complex concepts such as



Figure 1. Typical workstation of a professional trader. Credit: Photoagriculture/ Shutterstock.com

seasonal decomposition, exponential smoothing, and Auto Regressive Integrated Moving Average (ARIMA) models. Interestingly, machine learning methods have yet to significantly impact the time series domain, even for nonlinear tasks (e.g., [25, 26]).

This study is motivated by a financial application. Figure 1 shows a financial trader executing trades while observing financial time series images on their desktop screens. When it comes to financial time series, the data is consumed in its numeric form, but as shown in the figure, decisions are often augmented by visual representations. Recent studies [8, 7, 41] showed that computer-vision techniques and visual representations are effective in identifying and classifying trade patterns, as well as jointly predicting the price change direction of multiple assets. We follow these approaches and process time series data as images to produce corresponding forecast images of probabilistic future values.

We consider four different time series image data with various degrees of complexity: (i) multiscale synthetic harmonic data, (ii) mean-reverting synthetic data, (iii) real electrocardiogram (ECG) records, and (iv) real historical stock data. In each, the input data is processed as images, and we use convolutional autoencoders for image-to-image forecasting. We discuss ways to train the visual-forecasting

model and methods to assess visual forecast quality.

This work presents a few advantages. Visual time series forecasting is a data-driven non-parametric method, not constrained to a predetermined set of parameters. Thus, as shown when applied to the various datasets, the approach is flexible and adaptable to many data forms. This bears a stark contrast with classical time series forecasting approaches that are often tailored to the particularity of the data in hand. The main advantage of this method is that its prediction is independent of other techniques. This is important as it was repeatedly shown that an aggregate of independent techniques outperforms the best-in-class method (e.g., [13, 18, 15]). Also, visual predictions result in inherent uncertainty estimates about the point-wise forecast. In addition, financial time series data are often presented and act upon without having access to the underlying numeric information (e.g., financial trading using the smartphone Robinhood application). Thus, it seems viable to examine the value in inferring using images solely. Lastly, as will be discussed later on, we show that transforming the continuous numeric data to a discrete bounded space by means of visualization results in robust and stable predictions. Indeed, we show that visual forecasting outperforms the corresponding numeric forecasting baseline using the same kind of network.

In the following, we will discuss a few considerable technical difficulties. One caveat is that fine-grained time series prediction using images is data-hungry, which required us to use tens of thousands of examples. Another challenge is the representation form, as there are multiple ways to present time series data. This paper takes the most straightforward approach and analyzes 1-d data presented as a line plot, as discussed in the following sections.

## 2. Related Work

Time series forecasting is a standard statistical task that concerns predicting future values given all of the available information. Conventional forecasting tasks range from uncovering simple periodic patterns to forecasting intricate nonlinear patterns. The prevailing and most widely used forecasting techniques include linear regression, exponential smoothing, and ARIMA (e.g., [13, 21, 26]). In recent years, modern approaches emerge as tree-based algorithms (e.g., random forest), ensemble methods (e.g., gradient boosting), neural network autoregression, and recurrent neural networks (e.g., [13]). These methods are useful for highly nonlinear and inseparable data but are often considered less stable than the more traditional approaches (e.g., [21]).

Researchers recently studied the value of aggregating traditional statistical approaches and machine learning methods to increase prediction accuracy [40, 29, 34]. Results show that such ensembles achieve the best-in-class ac-

curacy for both point-wise predictions and confidence intervals about the forecast [26].

In the last few years, deep learning approaches began to be applied in the domain of time series analysis, for forecasting [33, 14, 4, 35], as well as unsupervised approaches for pre-training, clustering, and distance calculation [1, 28, 36, 38]. The common theme across these works is their use of stacked autoencoders (with different variations - vanilla, convolutional, recurrent, etc.) on numeric time series data. Autoencoders have also shown promise in the computer vision domain across tasks as image denoising [3, 17], image compression [2], and image completion and in-painting [27, 24].

This paper follows these studies and presents a new perspective on numerical time series forecasting by transforming the problem completely into the computer-vision domain. We convert the input data to images and build a network that outputs time series prediction images. To the best of our knowledge, this is the first study that aims at explicit visual forecasting of time series data as plots. Previous researches leveraged computer vision for time series data but focused on classifying trade patterns [8, 9], numeric forecast [7], learning weights to combine multiple statistical forecasting methods [23], and video prediction for multivariate economic forecasting [41]. We follow up on these approaches but focus on an explicit regression-like image prediction task.

## 3. Datasets

This paper uses four datasets, two synthetic and two real, with varying degrees of periodicity and complexity to examine the utility of forecasting using images.

### 3.1. Synthetic Data

We generate two different series for the synthetic datasets: multi-periodic data sampled from harmonic functions and mean-reverting data generated following the Ornstein–Uhlenbeck process.

#### 3.1.1 Harmonic data

The first dataset is derived synthetically and is designed to be involved but still with a prominent, repeated signal. We synthesized the time series  $s_t$  with a linearly additive two-timescale harmonic generating function,

$$s_t = (A_1 + B_1 t) \sin(2\pi t/T_1 + \phi_1) + (A_2 + B_2 t) \sin(2\pi t/T_2 + \phi_2),$$

where the time  $t$  varies from  $t = 1$  to  $t = T$ , and  $T$  denotes the total length of the time series. The multiplicative amplitudes  $A_1$  and  $A_2$  are randomly sampled from a Gaussian distribution  $\mathcal{N}(1, 0.5)$ , while the amplitude of the

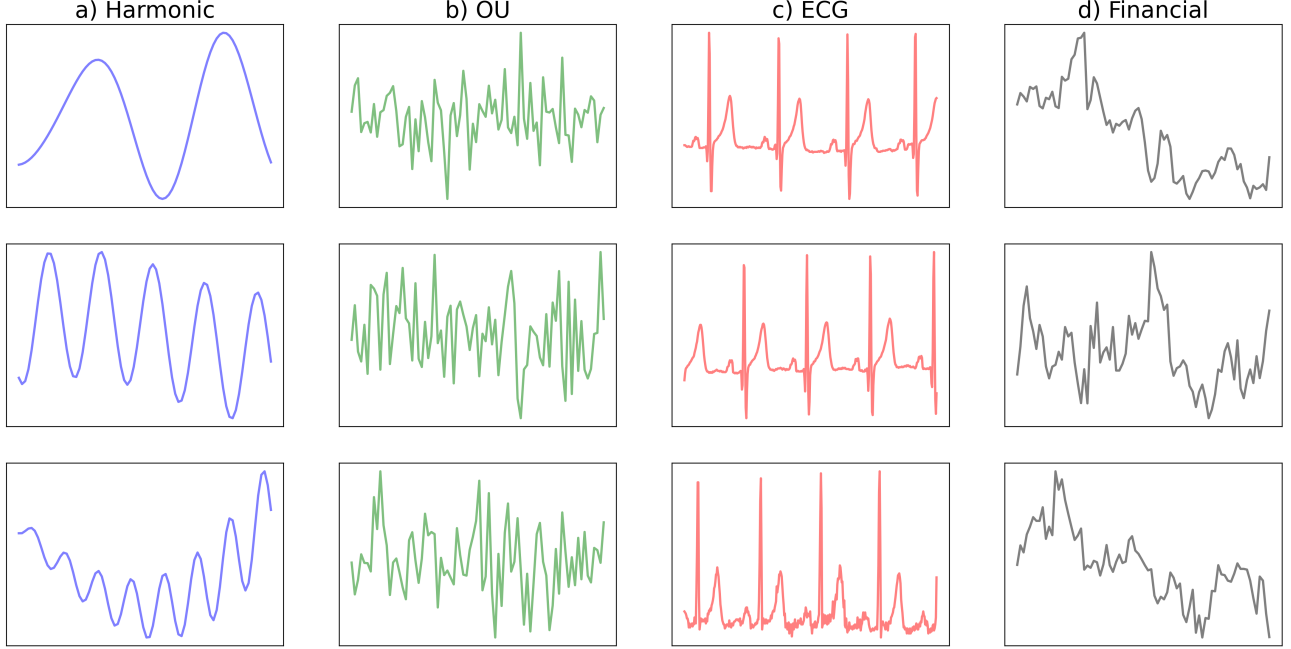


Figure 2. Sampled examples of the four datasets Harmonic, OU, ECG, and Financial.

linear trends  $B_1$  and  $B_2$  are sampled from a uniform distribution  $\mathcal{U}(-1/T, 1/T)$ . The driving time scales are short ( $T_1$ ) and long ( $T_2$ ) relative to the total length of  $T$ . Thus,  $T_1 \sim \mathcal{N}(T/5, T/10)$ , while  $T_2 \sim \mathcal{N}(T, T/2)$ . Lastly, the phase shifts  $\phi_1$  and  $\phi_2$  are sampled from a uniform distribution  $\mathcal{U}(0, 2\pi)$ . We generated and used 40,500 examples as a train set, 4,500 for the validation set, and 15,000 for the test set. Each time series differ concerning the possible combination of tuning parameters. Panel a) in Figure 2 shows three sampled examples of the harmonic data and it is easy to see that the synthetic time series consist of two time-scales: short oscillations that are composed on a much longer wave trains.

### 3.1.2 OU Data

We synthesized mean-reverting time series based on Ornstein–Uhlenbeck (OU) process as described in [5]. A mean-reverting time series tends to drift towards a fundamental mean value. We chose to synthesize the mean-reverting time series to resemble the characteristics of financial interest rates or volatility. OU’s stochastic nature makes it noisy on fine scales but predictable on the larger scale, which is the focus of this study. Specifically, we generated the OU dataset following the equation adopted from [5] with,

$$s_t \sim \mathcal{N}(\mu + (s_{t-1} - \mu)e^{-\gamma t}, \frac{\sigma^2}{2\gamma}(1 - e^{-2\gamma t})),$$

where  $\mu$  is the mean value that the time series reverts back to, and  $s_0$  starts at  $\mu$ . We used mean reversion rate  $\gamma \sim$

$\mathcal{N}(8e^{-8}, 4e^{-8})$  with units  $\text{ns}^{-1}$ , and a volatility value  $\sigma \sim \mathcal{N}(1e^{-2}, 5e^{-3})$ . Overall, we generated the time series by sampling  $s_t$  at every minute. We generated and used 45,000 examples as a train set, 5,000 for the validation set, and 15,000 for the test set. Similar to the Harmonic data, each time series differ concerning the possible combination of tuning parameters. Figure 2(b) shows three samples of the OU data. One can see that the OU data tend to be noisy with uncorrelated ups and downs, but on larger scales, the data is concentrated in the middle of the image as values drift toward the mean due to its reversion constraint.

## 3.2. Real Data

Along with the synthetically generated data, we use two real-world time series datasets.

### 3.2.1 ECG data

The ECG data is measured information from 17 different people adopted from MIT-BIH Normal Sinus Rhythm Database [16]. We curated 18 hours of data for each subject after manually examining the data’s consistency and validity by analyzing the mean and standard deviation of the time series data for each subject (not shown). For each subject, we consider a segment of 3.2 seconds (corresponding to 400 data points) sampled randomly from the data. 13 out of the 17 subjects are used a training data while the other 4 are used as out-of-sample testing data. Overall, we sampled 40,950 examples for the training set, while from the test data, we sampled 4,550 as a validation set and 14,000

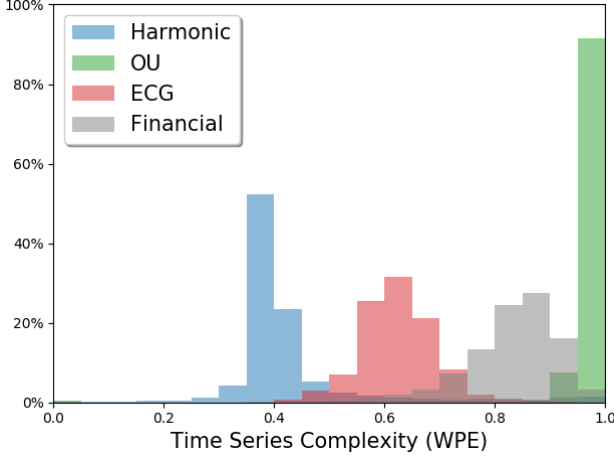


Figure 3. Distribution of dataset’s complexity measured using WPE.

as a test set. Panel c) in Figure 2 shows three sampled examples of the ECG data. One can see that the data has prominent spikes about every second, which makes the data predictable. However, there is noticeable noise between spikes that is much harder to predict.

### 3.2.2 Financial data

The last dataset is financial stock data from Yahoo! Finance. The data consists of daily Adjusted Close values of stocks that contributed to the S&P-500 index since 2000. Each time series segment consists of 80 days and is standardized by subtracting the mean and dividing by the standard deviation for each segment separately. For the train data, we sampled information randomly from the year 2000 to 2014, while for the test, we sampled information from 2016 to 2019. Overall, we sampled 38,173 examples as a training set, while from the test data, we sampled 4,242 as a validation set and 13,684 as a test set.

Panel d) in Figure 2 shows three sampled examples of the financial data. Here, one can see that the data is much less predictable than the previous three. Although financial data is persistent with sequentially related information, it is hard to spot repeated signals that will make the data predictable. Indeed, the prevailing theory of financial markets argues that markets are very efficient, and their future movements are notoriously hard to predict, especially given price information alone (e.g., [31]).

### 3.3. Complexity of Time-Series Data

To provide a reference for how the time series across our datasets vary, we measured the complexity of each with Weighted Permutation Entropy [11] (WPE). WPE measures the entropy of the ordinal patterns in time series data. In our experiments, we consider the ordinal patterns of each triplet  $(s_{t-1}, s_t, s_{t+1})$  along a given 1-d time series  $s$  where

$t$  stands for time. Short calculation shows that there can be  $\binom{3}{2} = 6$  possible ordinal patterns for each triplet. We normalize WPE into  $[0, 1]$ . The larger WPE, the more complex the data is.

As shown in Figure 3, we can see that the datasets cover a broad range of complexity. As expected, the simplest data is Harmonic with its deterministic periodicity. The ECG data is also periodic but more complex due to its irregularities between the spikes. The Financial data is not cyclic at all with almost random movement of fine scales, and, therefore, more complex than both the Harmonic and ECG. The OU data exhibits even more random oscillations and abrupt changes compared to other datasets, thus it is measured as the most complex dataset. However, on the larger scale, the OU data bounces around a hidden mean value with bounded noise, making it possible to predict future value *ranges*, as we will show later in Section 6.

## 4. Problem Statement

Given a time series signal, our goal is to produce a visual forecast of its future. We approach this problem by first converting the numeric time series into an image (as explained later in Section 5.1) and then producing a corresponding forecast image using deep-learning techniques.

Let  $X$  be the set of images of input time series signals, and  $Y$  be the set of corresponding forecast output images. The overlap constant  $c$  defines the overlap fraction between the input image  $x \in X$  and the forecast  $y \in Y$ , where  $c = 1$  implies  $x = y, \forall x \in X$ , and  $c = 0$  implies that  $x \cap y = \emptyset, \forall x \in X$ , i.e.,  $x$  and  $y$  are distinct. In our experiments, we use  $c = 0.75$  which means the first 75% of the forecast image  $y$  is simply a reconstruction of the later 75% of the input image  $x$ , and the rest 25% of  $y$  corresponds to visual forecasting of the future, as shown in Figure 8. We chose  $c = 0.75$  such that the reconstructed overlap region (first 75% in  $y$ ) serves as a sanity check on the effectiveness of a forecasting method, and the prediction region (later 25% in  $y$ ) provides forecasting into the near future.

## 5. Method

### 5.1. Data Preprocessing

Given a 1-d numeric time series  $S = [s_0, \dots, s_T]$  with  $s_t \in \mathbb{R}$ , we convert  $S$  into a 2-d image  $x$  by plotting it out, with  $t$  being the horizontal axis and  $s_t$  being the vertical axis<sup>1</sup>. We standardize each converted image  $x$  through following pre-processing steps. First, pixels in  $x$  are scaled to  $[0, 1]$  and negated (i.e.,  $x = 1 - x/255$ ) so that the pixels corresponding to the plotted time series signal are bright

<sup>1</sup>We plotted each time series  $S$  with bounded intervals. The interval for  $x$ -axis is  $[0 - \epsilon, T + \epsilon]$ , whereas the interval for  $y$ -axis is  $[\min(s_t) - \epsilon, \max(s_t) + \epsilon]$ , where  $\epsilon = 10^{-6}$ .



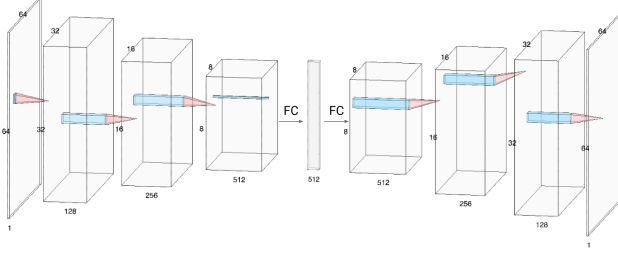


Figure 4. The architecture of undercomplete convolutional autoencoder network used in this study.

(values close to 1), whereas the rest of the background pixels become dark (values close to 0). Note that there can be multiple bright (non-zero) pixels in each column due to anti-aliasing while plotting the images.

Upon normalizing each column in  $x$  such that the pixel values in each column sum to 1, each column can be perceived as a discrete probability distribution. Columns represent the independent variable time, while rows capture the dependent variable: pixel intensity. The value of the time series  $S$  at time  $t$  is now simply the pixel index  $r(\text{row})$  at that time (column) with the highest intensity.

## 5.2. Image-to-Image Regression

As mentioned in Section 2, recent work has seen the extensive use of autoencoders in both the time series and computer vision domains. Following these, we extend the use of autoencoders to our image-to-image time series forecasting setting. We use a simplistic convolutional autoencoder to produce a visual forecast image with the continuation of an input time series image, by learning an undercomplete mapping  $g \circ f$ ,

$$\hat{y} = g(f(x)), \forall x \in X,$$

where the encoder network  $f(\cdot)$  learns meaningful patterns and projects the input image  $x$  into an embedding vector, and the decoder network  $g(\cdot)$  reconstructs the forecast image from the embedding vector. We purposely do not use sequential information or LSTM cells as we wish to examine the benefits of framing the regression problem in an image setting.

We call this method **VisualAE**, the architecture for which is shown in Figure 4. We used 2D convolutional layers with a kernel size of  $5 \times 5$ , stride 2, and padding 2. All layers are followed by ReLU activation and batch normalization. The encoder network consists of 3 convolutional layers which transform a  $64 \times 64 \times 1$  input image to  $8 \times 8 \times 512$ , after which we obtain an embedding vector of length 512 using a fully connected layer. This process is then mirrored for the decoder network, resulting in a forecast image of dimension  $64 \times 64$ . We will explain the loss function for training in detail in the next section.

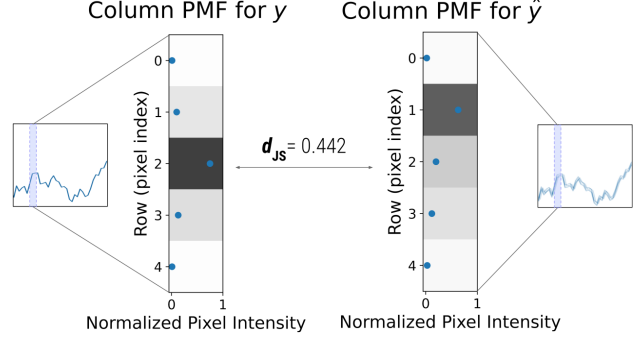


Figure 5. A depiction of comparison of two sample column probability distributions  $y = [0.01, 0.1, 0.75, 0.13, 0.01]$  and  $\hat{y} = [0.02, 0.63, 0.2, 0.12, 0.03]$ .

## 5.3. Loss Functions

One challenge with the converted time series images is that the majority of the information gets concentrated on fine lines, leaving most of the image blank. This is propagated downstream to the loss function that aims to quantify the dissimilarity of two sparse matrices.

We care about the likelihood of pixel intensity in a particular location (row) in each column of the forecast image. This can be achieved by leveraging metrics that compare two probability distributions. We do so in a column-wise manner: the loss  $L$  to compare target ground-truth (GT) image  $y$  with prediction image  $\hat{y}$  is the sum of column-wise distances between the two,

$$L(y, \hat{y}) = \sum_{i=1}^w d(y_i, \hat{y}_i),$$

where  $d$  is any distance measure between two distributions ( $y_i$  and  $\hat{y}_i$  in this case), and  $w$  is the width of images. This process is depicted in Figure 5.

Kullback-Leibler Divergence (KLD) (or relative entropy) is a well-established measure of comparing two probability distributions (e.g., [18]). It provides us a way of computing the distance from an *approximate distribution*  $Q$  to a *true distribution*  $P$ . KLD has been used extensively as a loss function in image classification and image generation, and it is commonly calculated as

$$D_{KL}(P||Q) = \mathbb{E}_P [\log(P/Q)].$$

In this study, following [20], we choose  $d$  to be the Jensen-Shannon Divergence (JSD), which is a symmetric, more stable version of KLD having the property that  $D_{JS}(P||Q) = D_{JS}(Q||P)$ . Here, JSD is computed as

$$D_{JS}(P||Q) = \frac{1}{2}D_{KL}(P||M) + \frac{1}{2}D_{KL}(Q||M)$$

where  $M = \frac{1}{2}(P + Q)$ .

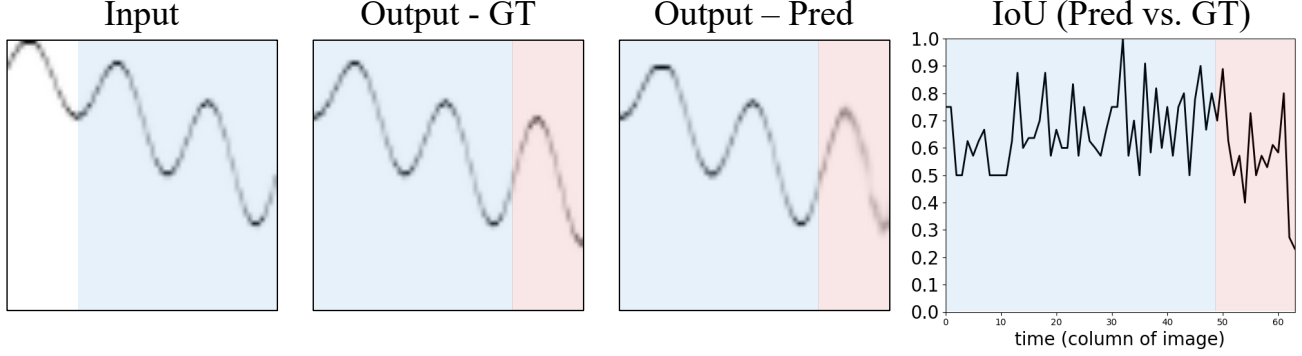


Figure 6. Illustration of the IoU metric for an example prediction on the Harmonic time series. *Blue*: overlap region between input and output images; *Red*: prediction region in output image.

## 6. Experiments

We experimented with four datasets: Harmonic, OU, ECG, and Financial, as they cover a wide range of complexity and predictability in time series data, as discussed in Section 3.3. In this study we use the PyTorch Lightning framework [30, 12] for implementation and Nvidia Tesla T4 GPUs in our experiments. We benchmark the proposed method against two baseline methods as we describe below.

**VisualAE**: This is the proposed method as discussed in Section 5.2. We train on images with size  $64 \times 64$ . We use a batch size of 128 and early stopping after 15 consecutive non-improving validation epochs to avoid overfitting during training. We start with a learning rate of 0.1, which is decayed by a factor of 0.1 (till  $1e-4$ ) after every 5 validation epochs with no improvement.

**NumAE**: We also train an autoencoder network to produce numeric forecasts of the original numerical time series signal. The numeric input and output time series are standardized using min-max normalization (with bounds obtained from the input to avoid leakage to future). The autoencoder is trained to predict the output time series by minimizing the Huber loss [19].

The architecture, though similar to Figure 4, is shallower (as the dimension of numeric input is much smaller than the images), and uses 1D convolutional layers of kernel size of  $5 \times 5$ , stride 2 and padding 2. All layers are followed by ReLU activation and batch normalization. The encoder part consists of a series of 2 convolutional layers (of  $T/2$  and  $T/4$  filters, where  $T$  is the length of the signal) and a fully connected layer, which gives us a latent representation of embedding length  $T/4$ . The decoder is a mirrored encoder.

We use a batch size of 128, along with a learning rate of 0.01 which is decayed by a factor of 0.1 after every 5 consecutive non-improving validation epochs. We also utilize early stopping, as described earlier.

**RandomWalk**: We used the random walk without drift model as a naive numeric forecasting baseline for comparison (e.g., [37]). Specifically, this model assumes that the

first difference of the time series data is not time-dependent, and follows a Gaussian distribution  $\mathcal{N}(0, \sigma)$ . Given a numeric input time series  $\{s_0, \dots, s_{t-1}, s_t\}$ , in order to predict  $\{s_{t+1}, \dots, s_{t+n}\}$ , we first estimate  $\sigma$  as

$$\sigma = \sqrt{\frac{t}{t-1} \mathbb{E}_{i=1}^t [(s_i - s_{i-1})^2]}$$

and the prediction at future time  $t + k$  follows

$$s_{t+k} \sim \mathcal{N}(s_t, \sqrt{k}\sigma).$$

To compare the numeric predictions produced by **NumAE** and **RandomWalk** with the visual predictions from **VisualAE**, we transform the numeric predictions into images using the process described in Section 5.1. We demonstrate the proposed method **VisualAE** outperforming both baseline methods across all four datasets, as discussed later in this section.

### 6.1. Forecast Accuracy Metric

To evaluate the prediction accuracy, we need to measure the similarity between the predicted image and the ground-truth image. We do this by utilizing the Intersection-over-Union (IoU) metric, as commonly practiced in the object-detection literature [10, 32].

We compute IoU pairwise for each corresponding column in the ground-truth and predicted image. This is done by obtaining the 1D bounding boxes of non-zero pixels for both and then calculating IoU using these. Figure 6 illustrates an example of the IoU of a predicted image (generated by the proposed method) measured against the ground-truth image. On the left, we show the input and the ground-truth output image. The overlapping region (overlap ratio  $c = 0.75$ ) between input and output is marked in blue. We aim to forecast the last 25% of the output image (marked in red). On the right, we show the predicted image, with the first 75% region (in blue) reconstructs the input while the last 25% (in red) region is the visual forecast.

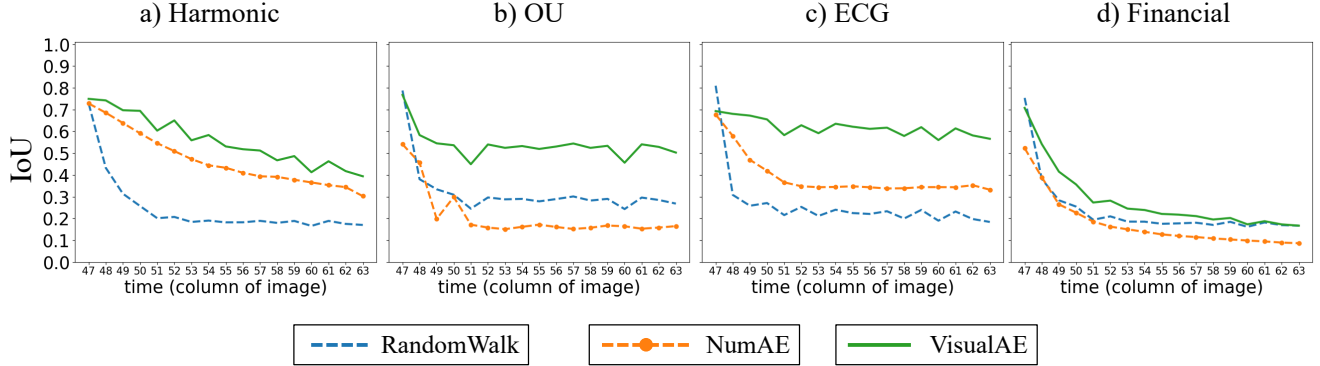


Figure 7. The averaged IoU accuracy of the proposed method **VisualAE** v.s. baseline methods **RandomWalk**, and **NumAE** measured in our test datasets. *x-axis*: index of image columns in the prediction region as annotated in red in Figure 6 and Figure 8.

The right-most panel in Figure 6 shows how IoU assesses the prediction quality. In the reconstruction area (in blue), the IoU measure is relatively stable, hovering at about 0.7. This number serves as a reference benchmark for an accurate prediction for this network and task. As expected, the IoU measure decreases as we move to the prediction region area marked in red. Here, the average IoU is about 0.4-0.5, which is about 30% lower than in the blue region.

## 6.2. Results

We demonstrate that the proposed method **VisualAE** outperforms the baseline methods **NumAE** and **RandomWalk**. As shown in Figure 7, **VisualAE** achieves higher IoU performance compared to the baseline methods across various datasets. For both **VisualAE** and **NumAE**, we averaged the IoU performance over five independently trained models with different random weight initializations. Please refer to Table 1 for more detail, where we summarized the mean and standard deviation of IoU scores averaged in the prediction region (as annotated in red in Figure 6). Similarly, we also provide the JSD scores (used as loss function during training) in Table 1 as a reference. However, we found JSD to be sensitive to small discrepancies between predicted and ground-truth images in general. Therefore, we focus our discussions on accuracy measured using IoU, which better reflects how well predicted images match ground-truth images visually. For the rest of this section, we will discuss these quantitative results in detail while referring to qualitative prediction examples from Figure 8.

**Cyclic Data:** Harmonic and ECG time series are more predictable than the other two datasets as they are dominated by cyclic patterns. Figure 8(a)(c) shows that **VisualAE** is able to capture these cyclic patterns well. Indeed, Figure 7 and Table 1 show that, **VisualAE** outperforms both baseline methods. In addition, the prediction accuracy of **VisualAE** degrades at a slower rate as time progress further into the future, especially for ECG data. For Harmonic data,

Dataset	Method	IoU	JSD
Harmonic	RandomWalk	$0.21 \pm 0.07$	$0.47 \pm 0.08$
	NumAE	$0.45 \pm 0.12$	$0.30 \pm 0.10$
	<b>VisualAE</b>	<b><math>0.55 \pm 0.13</math></b>	<b><math>0.25 \pm 0.12</math></b>
OU	RandomWalk	$0.29 \pm 0.06$	$0.36 \pm 0.04$
	NumAE	$0.19 \pm 0.05$	$0.51 \pm 0.04$
	<b>VisualAE</b>	<b><math>0.52 \pm 0.07</math></b>	<b><math>0.23 \pm 0.04</math></b>
ECG	RandomWalk	$0.23 \pm 0.05$	$0.43 \pm 0.04$
	NumAE	$0.37 \pm 0.06$	$0.34 \pm 0.07$
	<b>VisualAE</b>	<b><math>0.61 \pm 0.07</math></b>	<b><math>0.18 \pm 0.06</math></b>
Financial	RandomWalk	$0.20 \pm 0.09$	<b><math>0.46 \pm 0.07</math></b>
	NumAE	$0.15 \pm 0.10$	$0.57 \pm 0.08$
	<b>VisualAE</b>	<b><math>0.26 \pm 0.09</math></b>	$0.49 \pm 0.08$

Table 1. Mean IoU and JSD scores with standard deviation for the prediction region (annotated as red region in Figure 6 and Figure 8). Larger IoU (or lower JSD) score implies better prediction.

**VisualAE** performs slightly better than **NumAE**, while for ECG data, **VisualAE** performs significantly better. As seen in Figure 8(c), this is because of **VisualAE**’s ability to better recover the heart beat spikes. As a naive forecasting baseline, **RandomWalk** can only learn time-independent step-wise value changes, thus cannot model cyclic patterns.

**Random Synthetic Data:** It is hard to predict the exact daily changes in the OU data owing to the random process’ nature. However, over a larger scale, the OU data is predictable as a mean-reverting process. Visually, we expect majority of the values to concentrate around the mean value of the time series with some noise. Figure 8(b) shows that **VisualAE** concentrates on the hidden mean value, and was also able to partially recover the range of the noise. On the other hand, **NumAE** predicted the mean value as a steady line. Similarly, Figure 7 and Table 1 show that, on average, **VisualAE** outperforms both baseline methods.

**Financial Data:** Financial time series are the most challenging to forecast amongst the four datasets. According to

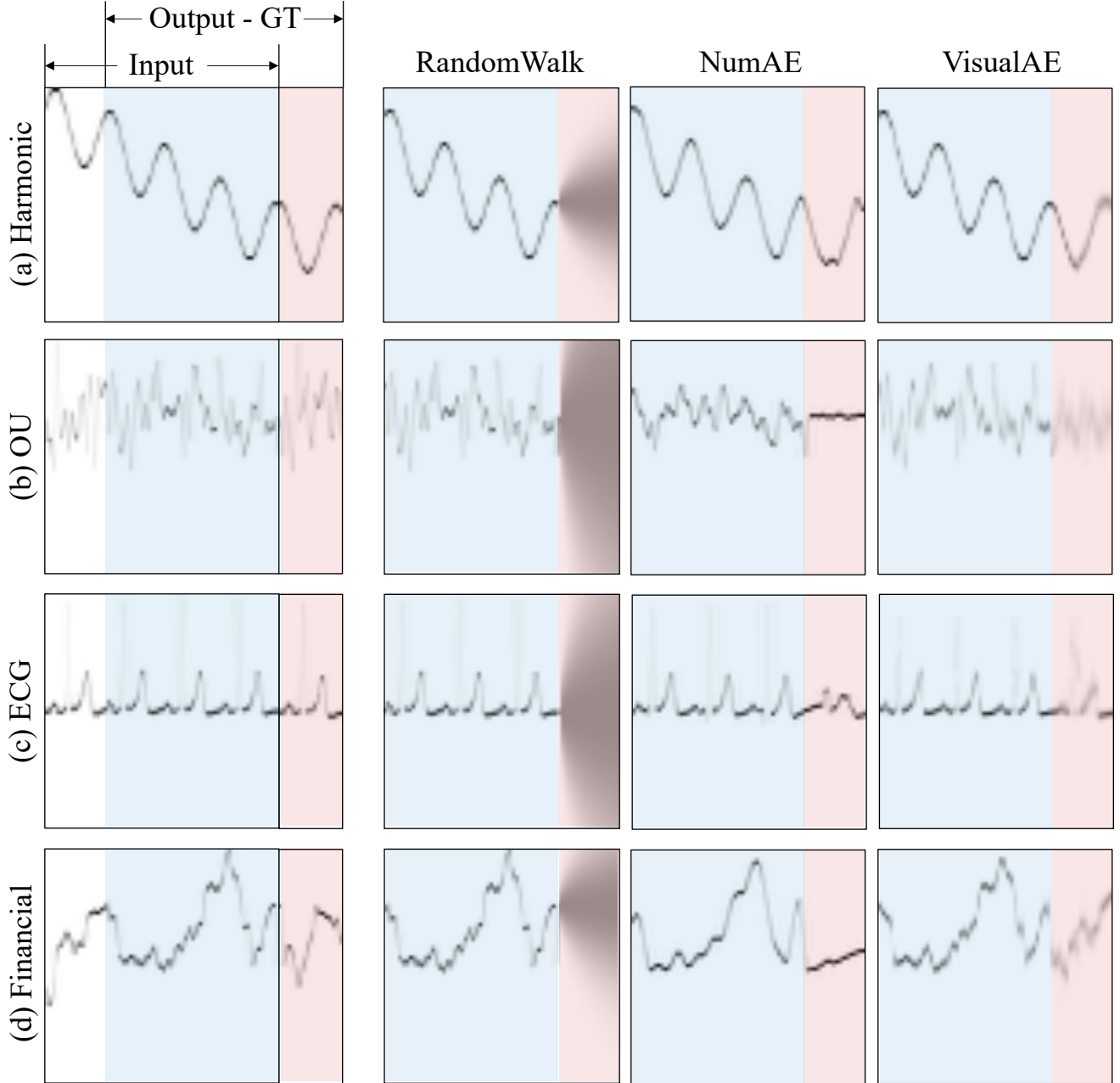


Figure 8. Example forecast predictions (out-of-sample) using the baseline methods **RandomWalk**, **NumAE**, and the proposed method **VisualAE**.

the prevailing literature (e.g., [31]), financial data is close to random on short scales and shows no apparent periodicity on large scales. Figure 8(d) shows that similar to the OU prediction, **NumAE** predicted the mean value with a weak linear trend, while **VisualAE** outperformed with a predicted curve that captures some of the finer details along with the overall nonlinear trend. Indeed, Figure 7 shows that, on average, **VisualAE** outperforms both baseline methods, at least for the first half of the prediction region. The margin

is small but notable and significant, and will be explored further in a follow-up study. It should be noted that, as expected for this data, the IoU scores degrade rapidly as time progresses further into the future. Both **NumAE** and **RandomWalk** underperform with the former underperforming the latter method after the first 25% of the time horizon. It is to be noted that our test set is relatively recent (2016-2019). Research indicates that the effectiveness of time series forecasting methods decreases over time (especially af-



ter 2009) when applied to financial stock data due to the increasing efficiency of the market and rising volumes of high-frequency trading [6]. This would also lend towards explaining the relatively lower performance on this dataset.

## 7. Summary and Conclusion

Time-series forecasting is one of the oldest disciplines in the sciences. Over the years, both academic researchers and industry practitioners found that classical statistical methods provide the most accurate and stable predictions, while recent advances in machine learning and deep learning have yet to significantly impact this field.

This study takes a novel approach and utilizes advances in computer vision to re-imagine the topic. We explored various datasets with varying degrees of complexity to demonstrate the utility of forecasting images by learning from a large pool of image pairs. We extended traditional deep learning architectures to this novel formulation by computing column-wise loss on pairwise probability mass functions.

We showed how to measure prediction performance using the IoU metric and demonstrated that forecasting using image data outperforms simple benchmarks and corresponding prediction applied to the numeric data. We suspect that the data’s visual representation exhibits robust and stable characteristics by transforming the continuous numerical information to a discrete and bounded space of pixel intensity and location.

This study is the first to use visual forecasting for time series prediction to the best of our knowledge. Our findings show promising results for both periodic information and irregular financial data.

## Disclaimer

This paper was prepared for information purposes by the Artificial Intelligence Research group of J. P. Morgan Chase & Co. and its affiliates (“J. P. Morgan”), and is not a product of the Research Department of J. P. Morgan. J. P. Morgan makes no representation and warranty whatsoever and disclaims all liability, for the completeness, accuracy or reliability of the information contained herein. This document is not intended as investment research or investment advice, or a recommendation, offer or solicitation for the purchase or sale of any security, financial instrument, financial product or service, or to be used in any way for evaluating the merits of participating in any transaction, and shall not constitute a solicitation under any jurisdiction or to any person, if such solicitation under such jurisdiction or to such person would be unlawful.

©2020 J. P. Morgan Chase & Co. All rights reserved.

## References

- [1] Abubakar Abid and James Y Zou. Learning a warping distance from unlabeled time series using sequence autoencoders. In *Advances in Neural Information Processing Systems*, pages 10547–10555, 2018. 2
- [2] Pinar Akyazi and Touradj Ebrahimi. Learning-based image compression using convolutional autoencoder and wavelet decomposition. In *Proceedings of the IEEE/CVF Conference on Computer Vision and Pattern Recognition (CVPR) Workshops*, June 2019. 2
- [3] Guillaume Alain and Yoshua Bengio. What regularized autoencoders learn from the data-generating distribution. *The Journal of Machine Learning Research*, 15(1):3563–3593, 2014. 2
- [4] Wei Bao, Jun Yue, and Yulei Rao. A deep learning framework for financial time series using stacked autoencoders and long-short term memory. *PloS one*, 12(7):e0180944, 2017. 2
- [5] David Byrd. Explaining agent-based financial market simulation. *arXiv preprint arXiv:1909.11650*, 2019. 3
- [6] David Byrd and Tucker Hybinette Balch. Intra-day equity price prediction using deep learning as a measure of market efficiency. *arXiv preprint arXiv:1908.08168*, 2019. 9
- [7] Naftali Cohen, Tucker Balch, and Manuela Veloso. The effect of visual design in image classification. *arXiv preprint arXiv:1907.09567*, 2019. 1, 2
- [8] Naftali Cohen, Tucker Balch, and Manuela Veloso. Trading via image classification. *arXiv preprint arXiv:1907.10046*, 2019. 1, 2
- [9] Bairui Du and Paolo Barucca. Image processing tools for financial time series classification. *arXiv preprint arXiv:2008.06042*, 2020. 2
- [10] Mark Everingham, Luc Van Gool, Christopher KI Williams, John Winn, and Andrew Zisserman. The pascal visual object classes (voc) challenge. *International journal of computer vision*, 88(2):303–338, 2010. 6
- [11] Bilal Fadlallah, Badong Chen, Andreas Keil, and José Príncipe. Weighted-permutation entropy: A complexity measure for time series incorporating amplitude information. *Physical Review E*, 87(2):022911, 2013. 4
- [12] WA Falcon. Pytorch lightning. *GitHub. Note: <https://github.com/PyTorchLightning/pytorch-lightning>*, 3, 2019. 6
- [13] Jerome Friedman, Trevor Hastie, and Robert Tibshirani. *The elements of statistical learning*. Springer series in statistics New York, 2001. 2
- [14] Andre Gensler, Janosch Henze, Bernhard Sick, and Nils Raabe. Deep learning for solar power forecasting—an approach using autoencoder and lstm neural networks. In *2016 IEEE international conference on systems, man, and cybernetics (SMC)*, pages 002858–002865. IEEE, 2016. 2
- [15] Aurélien Géron. *Hands-on machine learning with Scikit-Learn, Keras, and TensorFlow: Concepts, tools, and techniques to build intelligent systems*. O’Reilly Media, 2019. 2

- [16] Ary L Goldberger, Luis AN Amaral, Leon Glass, Jeffrey M Hausdorff, Plamen Ch Ivanov, Roger G Mark, Joseph E Mietus, George B Moody, Chung-Kang Peng, and H Eugene Stanley. Physiobank, physiotoolkit, and physionet: components of a new research resource for complex physiologic signals. *circulation*, 101(23):e215–e220, 2000. [3](#)
- [17] Lovedeep Gondara. Medical image denoising using convolutional denoising autoencoders. In *2016 IEEE 16th International Conference on Data Mining Workshops (ICDMW)*, pages 241–246. IEEE, 2016. [2](#)
- [18] Ian Goodfellow, Yoshua Bengio, Aaron Courville, and Yoshua Bengio. *Deep learning*. MIT press Cambridge, 2016. [2](#), [5](#)
- [19] Trevor Hastie, Robert Tibshirani, and Jerome Friedman. *The Elements of Statistical Learning*. Springer Series in Statistics. Springer New York Inc., New York, NY, USA, 2001. [6](#)
- [20] Ferenc Huszár. How (not) to train your generative model: Scheduled sampling, likelihood, adversary? *arXiv preprint arXiv:1511.05101*, 2015. [5](#)
- [21] Rob J Hyndman and George Athanasopoulos. *Forecasting: principles and practice*. OTexts, 2018. [1](#), [2](#)
- [22] R Krispin. Hands-on time series analysis with r: Perform time series analysis and forecasting using r, 2019. [1](#)
- [23] Xixi Li, Yanfei Kang, and Feng Li. Forecasting with time series imaging. *Expert Systems with Applications*, 160:113680, 2020. [2](#)
- [24] Yijun Li, Sifei Liu, Jimei Yang, and Ming-Hsuan Yang. Generative face completion. In *Proceedings of the IEEE conference on computer vision and pattern recognition*, pages 3911–3919, 2017. [2](#)
- [25] Spyros Makridakis, Evangelos Spiliotis, and Vassilios Assimakopoulos. The m4 competition: Results, findings, conclusion and way forward. *International Journal of Forecasting*, 34(4):802–808, 2018. [1](#)
- [26] Spyros Makridakis, Evangelos Spiliotis, and Vassilios Assimakopoulos. The m4 competition: 100,000 time series and 61 forecasting methods. *International Journal of Forecasting*, 36(1):54–74, 2020. [1](#), [2](#)
- [27] Xiao-Jiao Mao, Chunhua Shen, and Yu-Bin Yang. Image restoration using convolutional auto-encoders with symmetric skip connections. *arXiv preprint arXiv:1606.08921*, 2016. [2](#)
- [28] S Mostafa Mousavi, Weiqiang Zhu, William Ellsworth, and Gregory Beroza. Unsupervised clustering of seismic signals using deep convolutional autoencoders. *IEEE Geoscience and Remote Sensing Letters*, 16(11):1693–1697, 2019. [2](#)
- [29] Ping-Feng Pai and Chih-Sheng Lin. A hybrid arima and support vector machines model in stock price forecasting. *Omega*, 33(6):497–505, 2005. [2](#)
- [30] Adam Paszke, Sam Gross, Francisco Massa, Adam Lerer, James Bradbury, Gregory Chanan, Trevor Killeen, Zeming Lin, Natalia Gimelshein, Luca Antiga, et al. Pytorch: An imperative style, high-performance deep learning library. In *Advances in neural information processing systems*, pages 8026–8037, 2019. [6](#)
- [31] Lasse Heje Pedersen. *Efficiently inefficient: how smart money invests and market prices are determined*. Princeton University Press, 2019. [4](#), [8](#)
- [32] Hamid Rezaatoughi, Nathan Tsoi, JunYoung Gwak, Amir Sadeghian, Ian Reid, and Silvio Savarese. Generalized intersection over union: A metric and a loss for bounding box regression. In *Proceedings of the IEEE Conference on Computer Vision and Pattern Recognition*, pages 658–666, 2019. [6](#)
- [33] Pablo Romeu, Francisco Zamora-Martínez, Paloma Botella-Rocamora, and Juan Pardo. Stacked denoising auto-encoders for short-term time series forecasting. In *Artificial Neural Networks*, pages 463–486. Springer, 2015. [2](#)
- [34] Ali Safari and Maryam Davallou. Oil price forecasting using a hybrid model. *Energy*, 148:49–58, 2018. [2](#)
- [35] Alaa Sagheer and Mostafa Kotb. Time series forecasting of petroleum production using deep lstm recurrent networks. *Neurocomputing*, 323:203–213, 2019. [2](#)
- [36] Alaa Sagheer and Mostafa Kotb. Unsupervised pre-training of a deep lstm-based stacked autoencoder for multivariate time series forecasting problems. *Scientific Reports*, 9(1):1–16, 2019. [2](#)
- [37] Steven E Shreve. *Stochastic calculus for finance II: Continuous-time models*, volume 11. Springer Science & Business Media, 2004. [6](#)
- [38] Neda Tavakoli, Sima Siami-Namini, Mahdi Adl Khanghah, Fahimeh Mirza Soltani, and Akbar Siami Namin. Clustering time series data through autoencoder-based deep learning models. *arXiv preprint arXiv:2004.07296*, 2020. [2](#)
- [39] Daniel S Wilks. *Statistical methods in the atmospheric sciences*, volume 100. Academic press, 2011. [1](#)
- [40] G Peter Zhang. Time series forecasting using a hybrid arima and neural network model. *Neurocomputing*, 50:159–175, 2003. [2](#)
- [41] Zeng Zhen, Tucker Balch, and Manuela Veloso. Deep video prediction for economic forecasting. *Submitted*, 2020. [1](#), [2](#)